eTransportation 22 (2024) 100356

Contents lists available at ScienceDirect

eTransportation

journal homepage: www.journals.elsevier.com/etransportation

Battery pack diagnostics for electric vehicles: Transfer of differential voltage and incremental capacity analysis from cell to vehicle level

Philip Bilfinger *, Philipp Rosner, Markus Schreiber, Thomas Kröger, Kareem Abo Gamra, Manuel Ank, Nikolaos Wassiliadis, Brian Dietermann, Markus Lienkamp

Technical University of Munich, School of Engineering & Design, Department of Mobility Systems Engineering, Institute of Automotive Technology, Boltzmannstr. 15, Garching, 85748, Bavaria, Germany

ARTICLE INFO

Dataset link: mediaTUM, FTM Github

Keywords:
Battery electric vehicles
Lithium-ion battery
Battery pack diagnostics
Differential voltage analysis
Incremental capacity analysis
Battery aging

ABSTRACT

Aging of lithium-ion battery cells reduces a battery electric vehicle's achievable range, power capabilities and resale value. Therefore, suitable characterization methods for monitoring the battery pack's state of health are of high interest to academia and industry and are subject to current research. On cell level under laboratory conditions, differential voltage and incremental capacity analysis are established characterization methods for analyzing battery aging. In this article, experiments are conducted on the battery electric vehicles Volkswagen ID.3 and Tesla Model 3, examining the transferability of differential voltage and incremental capacity analysis from cell to vehicle level. Hereby, the vehicles are monitored during AC charging, ensuring applicability in real-life scenarios. Overall, transferability from cell to vehicle level is given as aging-related characteristics can be detected in vehicle measurements. Hereby, loss of lithium inventory is identified as the primary cause for capacity loss in the usage time of these vehicles. Both methods have limitations, such as data quality restrictions or vehicle specific behavior, but are suitable as diagnostics tools that can enable a vehicle level state of health estimation.

1. Introduction

The market share of battery electric vehicles (BEVs) is exponentially increasing, with the European Union ambitiously aiming to reach 30 million zero-emission vehicles by the year 2030 to further electrify the mobility sector [1]. In these BEVs, the energy storage is mostly made up of heavy, voluminous and expensive lithium-ion battery (LIB) packs to satisfy range and power requirements [2]. However, throughout a vehicle's lifetime, the condition of the battery pack deteriorates due to aging, usually expressed by the battery pack's state of health (SOH) [3]. Hereby, a SOH decrease can be measured as a reduced capacity and an increase of the battery cells' inner resistance [4]. Aging is divided into calendar aging during resting periods of the battery and cycle aging when under load [4–6]. In real life applications both aging mechanisms occur simultaneously leading to complex aging patterns [7]. From a customer's point of view, aging materializes in reduced range and power capabilities [4]. Therefore, regular status updates of the battery pack are relevant for the driver or fleet operator [8]. Furthermore, operators of a BEV fleet are interested in the vehicles' individual SOH to detect outliers and utilize predictive maintenance methods like scheduling visits at the workshop for increased dispatchability [9]. Moreover, BEVs will also be available for sale second hand after their first usage phase. Potential buyers of second hand cars might refrain from purchase due to an unknown SOH [10,11]. Also, insurance companies are interested in the SOH to determine premiums or the payout in case of a battery failure, especially regarding warranty claims [8]. Furthermore, business decisions on either keeping, selling, replacing or recycling a BEV can be taken based on the current SOH [8]. Hence, as the battery pack in BEVs is a significant driver of costs, knowledge about its present SOH is mandatory and methods for vehicle level battery back diagnosis necessary [8].

There are many approaches for an in-situ and non-invasive characterization of individual LIB cells under laboratory conditions through established diagnostic load cycles. The most common are the galvanostatic intermittent titration technique (GITT), electrochemical impedance spectroscopy (EIS), hybrid pulse power characterization (HPPC) and voltage-capacity analysis [12]. The latter encompasses differential voltage analysis (DVA) [13–16] and incremental capacity analysis (ICA) [17–19] both analyzing full charge or discharge cycles at low currents. Both DVA and ICA have proven valuable for the characterization

* Corresponding author.
E-mail address: philip.bilfinger@tum.de (P. Bilfinger).

https://doi.org/10.1016/j.etran.2024.100356
Received 19 March 2024; Received in revised form 2 August 2024; Accepted 5 August 2024
Available online 6 August 2024

of battery cells, i.e. for aging studies [20–22], cell-to-cell classification [23,24] or for SOH estimation by machine learning methods [25]. On the vehicle level, however, there are few approaches to characterize aging in battery packs of BEVs [9]. This paper aims at examining the transferability of DVA and ICA onto the vehicle level.

1.1. Literature review

The following section summarizes publications in literature that investigate differential voltage (DV) and incremental capacity (IC) curves from charging cycles as a suitable method for vehicle level battery diagnosis. Schmitt et al. [26] reconstruct the voltage curve from partial charge cycles and perform DVA in different state of charge (SOC) ranges and varying C-rates. The study tests cells under laboratory conditions, simulating charging at an 11 kW alternating current (AC) charger motivating applicability on the vehicle level. With this method, degradation modes and the cell capacity can be estimated accurately going through a range of 20-70 % SOC and a low current of $C/30$ enabling a SOH estimation. Weng et al. [27] develop a battery simulation environment to examine the applicability of an ICA peak tracking method on a module with three parallel connected cells for SOH monitoring. Furthermore, they vary the capacities and inner resistances of these cells in the model to analyze their effect on features of interest (FOIs) in the IC curves. The method is validated using 30 modules in a laboratory environment. Krupp et al. [28] analytically and experimentally examine ICA in a module with series-connected cells. They conclude that features on cell level dilute on the module level, particularly when single cells in the module have strongly aged. Hence, outliers in the module can be detected. The results show that there can be differences in module level IC curves determined by the terminal voltage to superposed voltages measured for each cell on the battery management system (BMS).

Further publications analyze data from charging events in BEVs to derive vehicle level DV and IC curves. Wassiliadis et al. [2] overlay a DV curve from a small current lab measurement of a Volkswagen (VW) ID.3 cell onto an AC charging cycle on vehicle level. They notice that the vehicles' BMS restricts voltage limits, presumably for capacity retention, compared to cell measurements in the laboratory. Therefore, shifting is necessary to align the vehicle to cell DV curve. Characteristics from the cell DVA then match adequately to the vehicle DVA, enabling the estimation of the cell's chemistry by comparison to literature findings. The same test set up was applied by Rosenberger et al. [29] with a Tesla Model 3 comparing the DV curves shortly after purchase to a measurement conducted after two years of utilization. Shifts of peak positions in the cell DV curves are observable, possibly due to increasingly deviating aging states of the cells. Furthermore, it is estimated that the measurable capacity loss of the battery pack is attributable to the loss of lithium inventory (LLI). Schaltz et al. [10,11] transfer ICA from cell to pack level for a BMW i3 and Nissan Leaf. In their study, characteristics from cell level ICA such as peaks and valleys generally match with measurements from the vehicle level, with small differences notable. A SOH definition is proposed by calculating a charged capacity within a fixed voltage range, due to BMS voltage limits prohibiting full capacity measurement. Furthermore, FOIs from the cell level ICA are correlated with the SOH and evaluated by FOIs from the vehicle ICA, showing a suitable match. She et al. [30] analyze partial charging cycles from 14 electric buses with a lithium iron phosphate (LFP) chemistry over a period of 14 months. Hereby, they extract the height of an IC peak as a FOI for each cycle that declines with increasing mileage. A radial basis function neural network is trained to predict the peak value from statistical features derived from the charging cycles. In a subsequent publication She et al. [31] extract the same IC peak for 12 BEVs and match this FOI with cell measurements. Furthermore, this vehicle level feature is evaluated by a cell level SOH estimator.

The excerpt of publications demonstrates that research increasingly focuses on battery diagnostics for BEVs. However, vehicle level diagnostics is often a motivation for cell level studies, simulated by battery pack models or examined by few inter-connected cells in the lab. Very few publications perform actual measurements on BEVs and either investigate by DVA or ICA. Especially FOI from IC curves are often subject to pure statistical analysis. Furthermore, data quality constraints in BEVs have not been examined, and a comparison of whether DVA or ICA is more suitable for vehicle level aging diagnosis is pending. Therefore, this paper addresses these research gaps by examining the transferability and applicability of both DVA and ICA on the vehicle level by focusing on standardized AC charging procedures and data quality constraints. Experiments are set up to compare cell level FOI associated with aging in LIBs to FOI on the vehicle level for two state of the art BEVs – the 2021 VW ID.3 and 2020 Tesla Model 3. Aging is assessed for both vehicles by DVA and ICA after a utilization period of two years. The overall goal is to further progress the technological readiness level of both DVA and ICA as vehicle level battery pack diagnosis methods.

1.2. Contributions

The scientific contributions of the underlying article are summarized as follows:

(a) Applicability of DVA and ICA on vehicle level
The process of applying DVA and ICA on vehicle level is extensively investigated by two BEVs, with different energy levels, cell chemistries, cell formats and battery pack configurations. Data quality constraints, as well as the influence of charging profiles on the utilization of both methods are examined.

(b) Transfer of DVA and ICA from cell to vehicle level
Additional cells from the vehicles under study are acquired and measured in a battery lab. A comparison is drawn by mapping DV and IC curves from cell to vehicle level measurements and analyzing the transferability of characteristic features.

(c) Aging diagnostics on vehicle level by DVA and ICA
The vehicles under study are compared by an initial measurement after purchase, to a state after two years of utilization. The objective is to evaluate FOIs that correlate with aging on cell level on their suitability as FOIs on vehicle level.

(d) Open access to all experimental data and code
A repository with data from the examinations is published openly with this article. This includes all time series of the measurements from the vehicles, as well as the code for processing the data.

1.3. Layout of the article

The further structure of the article is as follows: Section 2 briefly describes both principles of DVA and ICA. Section 3 describes the vehicles under study and the measurement procedures for obtaining data from small current charging cycles on vehicle and cell level. Section 4 shows the examination results of the following aspects, as shown in Fig. 1, with Section 4.1 investigating the effect of charging protocols on DV and IC curves from cell level measurements. The data quality of vehicle level measurements is analyzed in Section 4.2. The transfer of DVA and ICA from cell to vehicle level is portrayed in Section 4.3. Based on this, Section 4.4 discusses vehicle level degradation diagnostics to estimate the vehicles' SOH and Section 4.5 the influence of different BMS software versions. Section 5 summarizes the findings and Section 6 provides an outlook for further research.

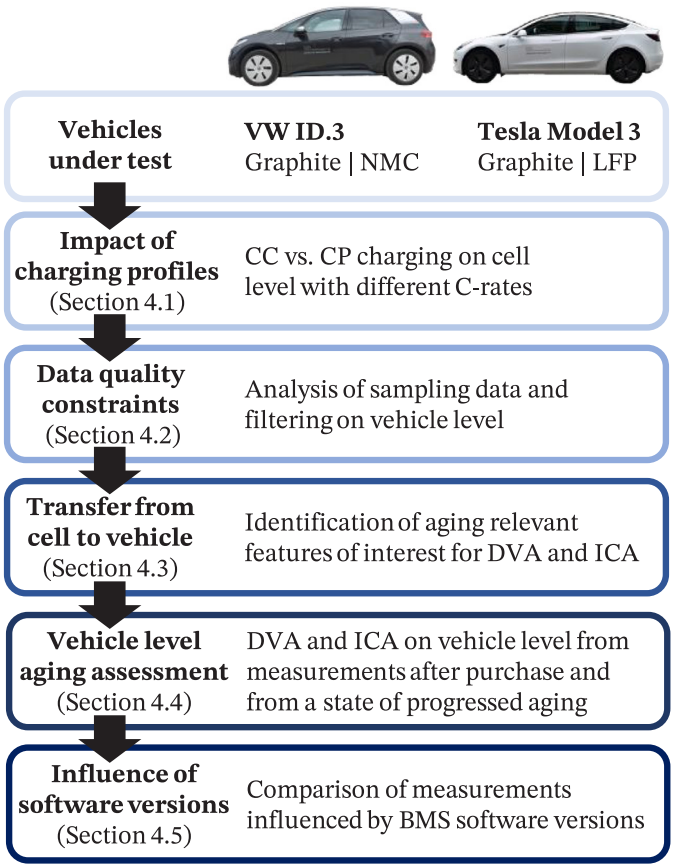

Fig. 1. Layout of the examined experiments in this article. The examinations are comprised of cell level as well as vehicle level measurements.

2. Fundamentals

Battery diagnosis with DVA and ICA analyzes the gradients of the voltage U and capacity Q signals from dis-/charging cycles by differentiation. Here, only charging is considered, as it is simpler to apply on the vehicle level and more reproducible, compared to draining the battery by driving on a chassis dynamometer. Furthermore, a small charging current or power is applied to reduce the excitation of overpotentials [32]. Depending on how the voltage and capacity signals are set into relation, results either in DV (Section 2.1) or IC (Section 2.2) curves. Both methods are widespread tools for in-situ characterization of battery cells with the main objective of extracting and analyzing insightful FOIs correlating with the SOH [18].

2.1. Differential voltage analysis

DV curves, as per Eq. (1), relate the differentiated voltage signal to the differentiated capacity signal. In other words, DVA enables the analysis on how the voltage changes due to an increase in transferred charge.

$$\mathrm{DV} = \frac{\mathrm{dU/dt}}{\mathrm{dQ/dt}} \approx \frac{\Delta U}{\Delta Q} \tag{1}$$

DVA enables insights into the stage transitions of the cells' electrodes at different lithiation levels [13]. Lithiation during charging describes the intercalation of lithium-ions into the negative electrode (NE), respective deintercalation from the positive electrode (PE), changing the electrodes' potential [13]. By definition, the open circuit voltage (OCV) of a LIB is the difference between the electrodes' open circuit potentials (OCPs) shown in Fig. 2(a). Accordingly, the difference between the electrodes' DV curves equates to the full cell (FC) DV curve, defined in Eq. (2).

$$\mathrm{DV_{FC}} = \mathrm{DV_{PE}} - \mathrm{DV_{NE}} \tag{2}$$

Detecting characteristic peaks in DV curves indicate the presence of a single phase inside one of the electrodes that can mostly be unambiguously assigned to either the PE or NE [13–16]. This is exemplary shown with halfcell data from the VW ID.3 (nickel-cobalt-manganese-oxide (NMC)/graphite) cell under study in Fig. 2(b). The peaks 4L, 3L and 2L are associated with liquid-like (L) intercalation stages of graphite electrodes and are named according to the number of empty graphite layers between fully lithiated layers [33]. Another dominant graphite characteristic is the stage 2 peak with no assumed in-plane order [26,33]. These graphite peaks are apparent in all cell chemistries with graphite in the NE which make up around 90 % of all LIBs [34]. Characteristic FOIs in this specific NMC chemistry are peaks H1, H2, and M, where the former two denote to a hexagonal and the latter a monolithic lattice structure. [35,36]. These features are less pronounced, due to the relatively low nickel content in this composition ($LiNi_{0.65}Mn_{0.2}Co_{0.15}O_2$) [37]. Ank et al. [38] provide a DV curve of a nickel rich NMC cell, where these characteristics are visible more clearly. Other PE chemistries, e.g. LFP do not exhibit any explicit features for DVA [39]. For deeper insights into phase transitions of common LIB active material compositions, the interested reader is referred to further publications [33,35].

Throughout their lifetime, cells progressively age leading to a reduced capacity [4]. The origin of the capacity loss can furthermore be divided into the degradation modes loss of active material (LAM) and LLI. The former summarizes aging mechanisms taking place at the positive and negative electrode leading to a reduced capacity of lithiation, while the latter corresponds to the loss of cyclable lithium no longer available for charge transfer between the electrodes [4,40]. Tracking peaks by DVA throughout aging makes it possible to identify degradation modes by evaluating the electrode capacities at the NE (Q_{NE}) and PE (Q_{PE}) to determine LAM as shown in Fig. 2(b). LLI can be observed by the balancing between electrode capacities (Q_B). These FOIs are often integrated into SOH estimation techniques [41]. Further FOIs, such as the height of the 4L or stage 2 peak can indicate inhomogenities in the distribution of intercalated lithium in the NE [20].

For practical applications, the differentiation of voltage and capacity signals is often implemented using numerical approximation (illustrated by Δ in Eq. (1)), by either forward, backward or central difference schemes [42]. Alternatively, the current signal I can directly be inserted in the denominator, due to $\mathrm{dQ/dt} = \mathrm{I}$ [2]. Here, the DV curves are normalized by the nominal capacity Q_n, scaling the DV curve into a regime along the y-axis around 1 V independent of the nominal capacity. In a battery pack the DV curve is accordingly scaled by the number of series-connected cells. Normalization can therefore simplify the comparability between different cell sizes. During continuous charging, the absolute charge signal increases monotonically, so that $\Delta Q \neq 0$ holds and there is no division by zero. Typically, the DV curve is plotted against the transferred charge signal from a full charging measurement [13]. Alternatively, DV curves can be plotted against the SOC, which is the charge signal normalized by the maximum capacity available according to the present SOH. A disadvantage of these signals is that both are secondary quantities not directly measurable by a sensor, but are rather calculated through integration of the current signal as shown in Eq. (3).

$$\mathrm{Q} = \int_{t_0}^{t_1} \mathrm{I}\,\mathrm{dt} + \mathrm{Q_{offset}} \tag{3}$$

Hereby, a full charging cycle reflects the transferred charge from 0-100 % SOC and is evaluated from the lower to the upper cut-off voltage at a predefined current which is generally specified in the cell's datasheet. Hence, the capacity of a cell can reproducibly be calculated and the charge signal begins at zero. On the contrary, the transferred

charge in a partial charging scenario does not cover the same full SOC range. It can therefore be necessary to estimate an offset Q_{offset} in order to align (partial) charge measurements, e.g. by using a reference. Plotting the DV curves against the SOC signal is equally not optimal, as determining an absolute SOC is not trivial. Depending on the SOC estimation method, operational conditions (e.g. extreme temperatures or dynamic current loads), and differences in relaxation times can lead to estimation errors [43].

2.2. Incremental capacity analysis

The IC curve is defined as the inverse of the DV curve relating the differentiated charge to the differentiated voltage shown in Eq. (4) [18]. Thus, identified valleys in DV curves are peaks in IC curves, and vice versa, serving as FOIs. IC peaks give insights into the transition between electrode lithiation phases. IC curves are commonly plotted against the voltage signal which is a directly measured property, so that alignment is not necessary, which is an application advantage for vehicles under real operation conditions [18,44].

$$\mathrm{IC} = \frac{\mathrm{dQ/dt}}{\mathrm{dU/dt}} \approx \frac{\Delta Q}{\Delta U} = \frac{1}{\mathrm{DV}} \tag{4}$$

Inserting Eq. (2) into Eq. (4) makes clear that FOIs from the FC ICA are not additively superimposed characteristics from electrode ICAs, but rather result from convolution. Therefore, findings from ICA are harder to disaggregate and interpret [18]. Nevertheless, peak A in Fig. 2(a) can be associated with stage transitions at the NE, peak C from both electrodes and characteristics B and D with the PE [35,45,46]. The position of these peaks and plateaus (e.g. A–D) can be tracked as FOIs, as well as differences in peak heights (Δh), peak widths (Δw) or integrals between voltage boundaries ($\int$) schematically shown in Fig. 2(c). Clear statements regarding aging are often only possible by jointly analyzing multiple FOI and their relation to another [18].

During aging, the internal resistance of the cell gradually increases, e.g. through solid electrolyte interphase (SEI) formation. Following Ohm's law, a resistance increase leads to a voltage increase. Assuming a homogeneous resistance increase over the whole SOC range shifts the IC curve accordingly, as it is plotted against the voltage signal. This property can be detected as a FOI by ICA, e.g. by tracking peak positions throughout the aging process [41].

Normalizing IC curves by the nominal capacity as for DV curves is possible, but is omitted here as the unit $^1/_V$ is less intuitive. Some LIB chemistries (e.g. LFP) inhibit minimal voltage increases over broad SOC intervals. Differentiating the voltage signal at these plateaus leads to small differences in the denominator ($^1/_{\Delta U}$) yielding steep gradients in IC curves [18,47]. In turn, this imposes high demands on the data quality and sampling rate in order to capture the relevant characteristics for further interpretation.

3. Methodology

An introduction to the BEVs under study is presented in Section 3.1. Further, the test procedure (Section 3.2) and data acquisition (Section 3.3) are explained in detail. For a comparison, cell level measurements are conducted and described in Section 3.4.

3.1. Vehicles under test

The experimental vehicles in this paper include a VW ID.3 Pro and Tesla Model 3 Standard Range Plus. The exact specimens of the VW ID.3 was comprehensively investigated by Wassiliadis et al. [2] with an in-depth teardown of the powertrain and battery pack. All presented vehicles were purchased from a dealership so that they are unmodified mass-production vehicles and ensure an unbiased examination. The vehicles under study are briefly described with focus on battery pack specifications summarized in the Appendix in Table 1.

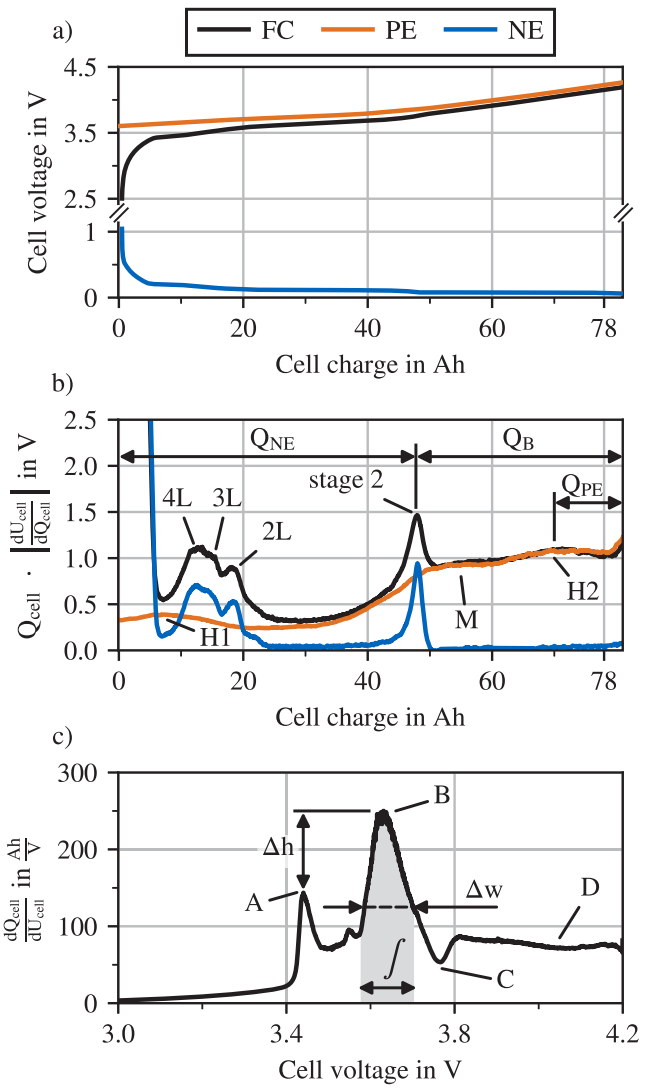

Fig. 2. Schematic half-cell measurements from three electrode cells [37] (a) Full-cell (FC) voltage curve from a $^C/_{50}$ charging cycle with a NMC cell resulting from the difference in positive electrode (PE) and negative electrode (NE) OCPs. (b) Full-cell and half-cell DV curves. Peaks associated with single phases in the electrodes are labeled, as well as the NE, PE and balancing (B) capacity. (c) The FC IC curve results from the convolution of electrode IC curves. Peaks are associated with stage transitions in the electrodes. Typical FOIs for aging analysis by ICA are visualized.

The examined 2021 VW ID.3 Pro (abbreviated as VW) is equipped with a 58 kWh battery pack. The battery pack architecture consists of nine modules connected in series, each of which contains 24 cells in a 12s2p configuration. On pack level, the voltage ranges from approx. 360-450 V [2]. The NMC pouch cells contain a PE composition with $LiNi_{0.65}Mn_{0.2}Co_{0.15}O_2$ and pure graphite (without silicon) for the NE [37].

The 2020 Tesla Model 3 Standard Range Plus, referenced as Tesla, comes with a 55 kWh battery pack and a voltage range of approx. 330-380 V [48]. This particular specimen is assembled with prismatic LFP cells in a 106s1p configuration [48]. The NE is composed of pure graphite without any silicon content [49].

3.2. Measurement procedure

To enable a fair comparison, it is necessary to set up the vehicle level measurements as similarly as possible to the cells measured in laboratory conditions, regarding both the testing procedure or ambient

conditions. Here, the small current measurement is set in the charging direction, as the procedure is simpler and reproducible during standardized AC charging. Discharging the vehicles on a chassis dynamometer in a continuous manner is also possible, but cumbersome.

The vehicles are fully discharged to 0 % SOC before the measurement. In the VW however, the SOC displayed in the user interface (UI) is offset by about 4 % compared to the SOC read from the BMS, presumably due to reserved capacity margins. Therefore, 0 % UI SOC is equivalent to 4 % BMS SOC. For the Tesla, the shift between BMS and UI equals 0.2 %. In the following, the SOC is solely based on the BMS data. Discharging the vehicles is a lengthy procedure, especially for the VW as driving is disabled at 4 % SOC. Full discharge is achieved using the heating, ventilation and air conditioning system similarly to Schaltz et al. [10,11] and Wassiliadis et al. [50], which takes multiple hours.

The vehicle level measurements are performed with the commercially available charging device Juice Booster 2 (Juice Technology, Switzerland [51]). Depending on the socket type (single/triple phase) and the current selection on the charger an AC power in the range of 1.4-22 kW is supplied. Here, a low charging current is preferred to achieve a quasi-stationary charging measurements and reduce the effect of inhomogeneity in the NE that can dilute FOIs for DVA and ICA [18,20]. Therefore, a maximum single phase charging current of 8 A is set by the Juice booster limiting the power supply to 1.84 kW. The vehicles are then fully charged in a temperature controlled environment at 20 °C until the vehicle terminates the charging session. Both vehicles offer power reduction options in the UI to reduce the stress on the battery which is additionally selected for all measurements. The energy content of the battery pack is evaluated by integrating the charging power as defined in Eq. (5).

$$E = \int_{t_0}^{t_1} P \, dt = \int_{t_0}^{t_1} U \, I \, dt \tag{5}$$

It is common in the literature to express currents by the C-rate for a better comparability between cell formats. The C-rate is defined as the current I related to the nominal capacity C_n as shown in Eq. (6) and often given in the unit $^1/h$ [52]. For constant current (CC) profiles the C-rate is constant and its reciprocal indicates the time span of a full charging cycle.

$$\text{C-rate} = \frac{I}{C_n} \tag{6}$$

However, in many vehicle applications not the current, but rather the power is the set property, e.g. for the demanded power in driving scenarios or when charging the vehicle using a constant power (CP) profile. The latter means that electrical power (P = U I) is held constant throughout the charging cycle. Hence, as the voltage in the battery pack increases, the current is reduced accordingly. In this case, the C-rate is not constant with the standard definition. Therefore, the E-rate is defined by Eq. (7) based on the charging power P in relation to the battery pack's net energy E_n [53].

$$\text{E-rate} = \frac{P}{E_n} \tag{7}$$

For simplicity and as both definitions express the same property, namely the time for a full charging cycle, the nomenclature here is reduced to the more custom C-rate. Hence, when comparing CC to CP measurements, it is made sure that the charging time (inverse of the C-rate or E-rate) is equal. Following this definition results in C-rates of $^C/_{45}$ for the VW and $^C/_{57}$ for the Tesla with the given charging power.

3.3. Data acquisition

For the Tesla, a controller area network (CAN) logger is connected to the vehicle, recording all bus traffic for later conversion to physical values through a .dbc file available on GitHub [54]. For the ID.3, however, unified diagnostic services (UDS) requests are sent through a self-built data logger [55] connected to the OBD II diagnostic interface to query individual values in a frequency of 1000 ms. Responses from the gateway board are requested by addressing the unique message identifiers (IDs) of the packs' voltage, current and SOC, additional to all cell voltages. The response frequency slightly deviates during and between measurements, presumably due to bandwidth limitations in the gateway board for handling requests. Practically, a sample of each requested signal is logged in a time span of approx. 10 s, leading to a sample frequency of 0.1 Hz. By analyzing the signals' discretization, an estimated resolution can be given for the pack voltage (±0.25 V) and pack current (±0.01 A). After completion of the measurement, the signals are synchronized onto a single time vector by interpolation. The interested reader is referred to Merkle et al. [56] for an in-depth descriptions of the data acquisition process.

3.4. Cell measurements

Additional battery cells from the vehicles under study are acquired for comparative cell level measurements. It is unknown how these modules were stressed beforehand, as they are not pristine specimens. Both cells are connected to channels in the MRS 6 V battery cycler manufactured by BaSyTec GmbH (Germany, ±600 A per channel) with a current and voltage resolution of ±300 mA and ±0.3 mV, respectively. During measurements, the cells are placed inside a VC^3 4100 thermal chamber by Vötsch GmbH (Germany) to ensure a constant ambient temperature during testing. The cell teardown and preparation for laboratory measurements is described closely by Wassiliadis et al. [2]. It is noted that the pouch cells in the VW are not disassembled from the module housing to sustain the original cell compression.

The cells are initially discharged to the lower cut-off voltage by a constant current constant voltage (CCCV) profile and subsequently relaxed for 2 h prior to the small current charging measurements for acclimation and relaxation effects to fade away. The cells are then charged until the upper cut-off voltage is reached either by a CC or CP pattern, depending on the examination. Furthermore, the charging current or power is chosen to match the vehicle level measurements. Datapoints are sampled at a rate of 1 s (1 Hz), or when a voltage delta of 4 mV is detected.

4. Results and discussions

Firstly, CC and CP charging profiles are compared on the cell level in Section 4.1. In Section 4.2, data quality of vehicle level measurements are examined. The transferability of the voltage curves, DVA and ICA from cell level to vehicle level is investigated in Section 4.3. Lastly, aging of the BEVs under study is examined in Section 4.4 and the influence of BMS software versions in Section 4.5.

4.1. Charging profiles

A CC profile is a typical charging profile for LIBs in lab tests holding the current constant throughout the entire charging session. Furthermore, the CC phase is often followed by a constant voltage (CV) phase to further charge the cell without exceeding the upper cut-off voltage limit. Out of necessity, e.g. energy conservation, however, a CP profile is common when charging BEVs at AC chargers. In terms of the calculation of DV and IC curves (Section 2), pure CC charging is favorable, as the derivative of the charge signal is constant ($^{dQ}/_{dt} = I = const.$), while only the voltage signal changes significantly. Distinct FOIs can therefore be unambiguously attributed to thermodynamic voltage changes only. Furthermore, dynamic effects due to changes in the current are mitigated. Here, the aim is to investigate effects on FOIs for DVA and ICA from CP charging data.

Fig. 3 compares CC and CP protocols for a single VW NMC pouch cell in the battery lab. Fig. 3(a) depicts the current profiles of a $^C/_{45}$ full range CC (1.7 A) and CP (6.6 W) charge with the current/power determined by Eq. (6) and Eq. (7). A second $^C/_6$ measurement with

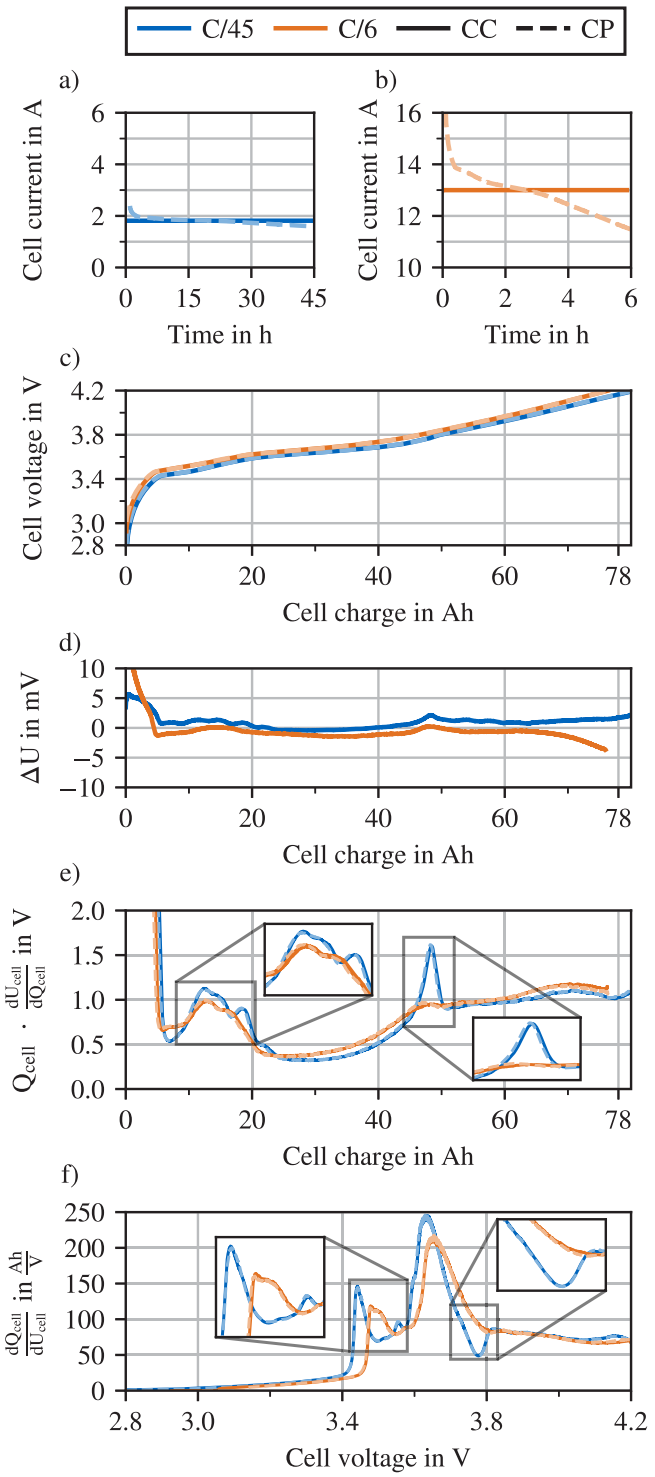

Fig. 3. Comparison of the effect of CC and CP protocols on FOIs for DVA and ICA. The measurements are conducted on the same VW NMC pouch cell in the battery laboratory. (a)/(b) Current and power profiles for a $C/45$ and $C/6$ charging measurement. (c) CC and CP voltage curves for both C-rates. (d) Voltage error between CC and CP measurements. (e)/(f) Associated CC/CP DV and IC curves.

a higher current/power (13 A/49.2 W) is shown in Fig. 3(b). All measurements are conducted between the voltage range from 2.8-4.2 V. The difference of the applied currents is the greatest at the beginning and end of charge with and maximum of 0.6 A and 3.1 A, respectively.

In Fig. 3(c), the corresponding $C/45$ and $C/6$ voltage curves are visualized. The effect of the higher current can be seen in the $C/6$ measurement as higher overpotentials shift the curve towards higher voltages. Therefore, the cut-off voltage termination criterion is reached sooner leading to a delta of 4 A h between measurements. However, CP and CC pseudo open circuit voltage (pOCV) data generally aligns well for both current levels evaluated by the voltage difference shown in Fig. 3(d). Overall, an absolute average difference of 1.1 mV, respective 1.3 mV is measured. The largest deviation between voltage signals is visible at the start and end of charge in the $C/6$ measurement following the CP current load.

To elaborate distinct differences in the charging protocols, DVA offers deeper insights shown in Fig. 3(e). The effects of higher C-rates can be seen more clearly in the close up plots where the $C/6$ measurement shows a dilution of features [57,58]. Especially the graphite peaks (4L, 3L, 2L and stage 2) dilute due to increased inhomogeneity of the lithium distribution in the NE, as diffusion processes take longer to equate for local lithium concentration gradients [20]. Similar findings can be seen in the IC plot in Fig. 3(f), where additionally the $C/6$ curve shifts to higher voltages due to more significant overpotentials from the higher C-rate.

With the insights from DVA and ICA, it seems as if neither the $C/45$, nor the $C/6$ CP measurement deviates strongly to their respective CC counterparts. When examining the close-ups, marginal differences can be seen between CP and CC measurements around areas where the voltage differentiates the most. For instance, the CP DV curve is below the CC DV curve in the $C/6$ measurement between 60-78 A h due to the decreasing current at this SOC interval. Nonetheless, both charging profiles make it possible to distinguish insightful FOIs from DVA and ICA so that CP measurements on vehicle level are not necessarily a drawback. Further measurements can be conducted at higher C-rates, but it is doubtful that the effect of a CP charging profile exceeds the influence of inhomogeneity imposed by increased C-rates.

4.2. Data analysis

The differentiation of sensor data, as necessary for DVA and ICA, amplifies noise in the derived signal, hampering the extraction of insightful features. Prefiltering the voltage and charge signals is therefore necessary to smooth the signals and reduce noise. Postfiltering DV and IC curves is often also required to enhance the visibility of FOIs. Care must be taken when smoothing the signals, as characteristics can be altered leading to false interpretations [18,44,59].

Fig. 4 depicts the vehicle level DV and IC curves from a $C/57$ charging measurement with the Tesla. The LFP cell in the Tesla is known for its flat voltage profile, i.e. showing small voltage increases over broad SOC intervals [60,61]. Capturing changes in the voltage and current signal is essential for calculating both methods, placing high quality demands on the sensors, especially for LFP cells, to provide sufficient resolution, precision and suppression of noise [18,47]. However, the data recorded from the vehicles under study originates from on-board sensors with unknown specifications. Therefore, the results shown for the LFP cell demonstrate an edgecase demanding high data quality and aims at investigating vehicle sensor requirements.

In Fig. 4(a), the raw DV curve is plotted where neither the voltage nor the capacity signal is prefiltered. For the sake of visibility only every 100th datapoint is shown and it is clear that no characteristics can be extracted out of this signal. The noise is visualized in a Bode plot in Fig. 4(b) up to the highest resolvable (Nyquist) frequency ($f_{nyquist} = 2 \cdot f_{sample}$), where the majority of high amplitude disturbances are discernible in the higher frequency regime ($\geq$ 1 mHz) of the signal. The same statements holds for the raw IC curve, calculated by the inverse of the DV curve, showing similar effects in Fig. 4(c) and (d). Hence, filtering vehicle data is essential and cannot be omitted.

A moving mean filter is applied to the charge and voltage signal in forward direction. The filter induced shift acts on the same timescale of

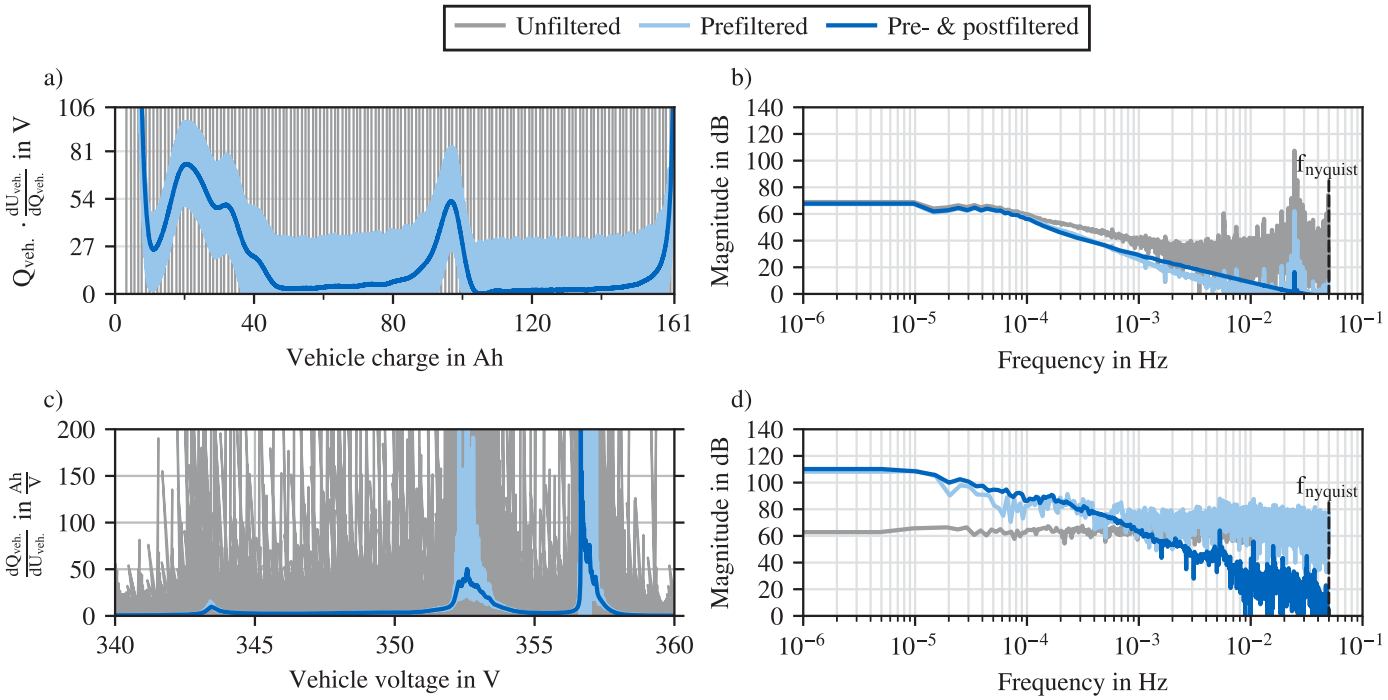

Fig. 4. Influence of filtering vehicle level DV and IC curves shown for a $C/57$ charging measurements with the Tesla. Tesla's LFP cells have a characteristic flat voltage profile placing high demands on the data quality. (a)/(c) DV and IC curves without filtering, prefiltering the voltage and capacity signals and additional postfiltering. (b)/(d) Corresponding Bode plots plotted against the frequency.

both signals which eventually cancels out deriving the DV or IC curves. It is noted that other authors directly filter the current signal instead of the charge signal [2]. However, numerically integrating the current to calculate the charge signal suppresses noise which in turn increases the effectiveness of the applied filter.

The window size of the filter is set to 1 % of datapoints, to standardize the filtering over measurements, C-rates and capacities. Such preprocessing already improves the effectiveness of DVA/ICA significantly reducing the influence of high frequency noise visible in the Bode plots. However, remaining amplified noise still makes extraction of distinct FOIs difficult. Furthermore, it becomes clear why extracting the IC curve from LFP cells is difficult, as the flat intervals in the voltage profile leads to sharp extrema. Additionally, a low voltage resolution yields unclear peaks as the voltage difference is close to zero and noise leads to $dU/dt \pm 0$. Postfiltering finally yields a DV curve suitable for FOI extraction further suppressing high frequency noise. To achieve that, the DV curve is again filtered by a moving mean filter with a window size of 1 % of datapoints in forward and backward direction to equalize filter induced shifts. Other filters, such as Gaussian filtering or Savitzky–Golay filters are examined in other publications [44,59]. The reason for calculating the IC curve from the inverse of the (postfiltered) DV curve is because filtering works more effective with smoother gradients, as steep gradients can falsely be evened out. Undefined values in the IC curve are subsequently deleted and outliers omitted through an interquartile range filter. The latter deletes datapoints with values outside the 5th to 95th percentile of ordered IC values.

Concerning data sampling, the sample rate is the only variable parameter during the vehicle measurements and is fixed to 10 s (sample frequency of 100 mHz). Undersampling a signal can lead to temporal aliasing which can distort and filter out FOIs [62]. This effect is examined by reducing the sample rate of the $C/57$ measurement above. Fig. 5(a) shows the DV curve with sample rates between 10-3600 s. The close-up plot focuses on the stage 2 peak which is relevant for calculating electrode capacities and evaluating lithiation in-homogeneity of the NE (Section 2.1). The sample rate is sufficiently high for a precise reconstruction, if this peak can be captured without distortion. Qualitatively, sample rates below 300 s (3.3 mHz) seem workable before the smooth curvature becomes edgy and reduces in height. A rule of thumb can be postulated by generalizing this sample rate with the applied C-rate that a sample point is necessary for a delta change in the capacity (CC charging) or energy (CP charging) of approx. 0.2 %. The distorted peak in Fig. 5(a) might exclude exact statements about battery internal processes, but the x-position of the peak can still be approximated as a FOI for all evaluated sample rates. Therefore, DVA is insensitive against these examined sample rates when examining the peak's x-position.

Fig. 5(b) and (c) depict the IC curves for sample rates 10-300 s and 900 s, respectively. As for DVA, a sample rate of 300 s is sufficient for resolving the curve. Lower sample rates however induce noise so that identifying peaks is ambiguous indicating that (LFP) ICA is more susceptible to the sample rate than DVA. Further IC curves are omitted, due to extreme noise.

As described above, these results show an edgecase of vehicle level DVA and ICA with LFP cells, due to the flat voltage profile. Nonetheless, the findings indicate that not necessarily the sample rate, but rather noise and the resolution of the sensors are limiting. It is shown that a sample point every 10 s is sufficient and even sample rates as low as 300 s between samples are possible for this C-rate. Overall, care must be taken when extracting FOIs, especially for ICA, as filtering is indispensable. Furthermore, DVA is more robust, as peaks identify voltage changes which are easier to resolve. Also, DV curves exhibit more moderate gradients, which are more forgiving in sampling and filtering requirements. Lower data quality does not hamper the approximation of peak position, e.g. for determining electrode capacities, whereas in-depth insights become difficult to examine. In contrast,

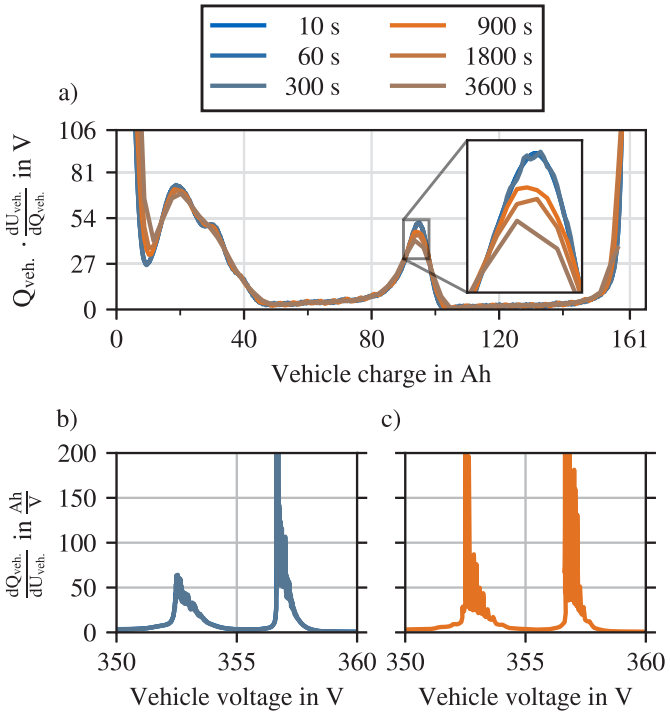

Fig. 5. Influence of reducing the sample rate of a $^{C}/_{57}$ Tesla measurement. (a) DV curves with sample rates 10-3600 s. A sample rate of 300 s (3.33 mHz) is sufficient for capturing the stage 2 peak smoothly. (b)/ (c) IC curves for sample rates 10-300 s and 900 s, respectively.

peaks in IC curves resemble plateaus in the voltage curve requiring a high resolution by appropriate sensors where noise further complicates the calculation. IC curves can nevertheless be calculated and yield clear results, especially for cell chemistries with no flat voltage intervals like the NMC cells in the VW shown in Fig. 2(c). Hence, knowing a BEVs cell chemistry and/or sensor specifications can determine if ICA is suitable for vehicle level diagnostics or not. If high quality data cannot be ensured, it is recommended to rather observe trends in peak movement instead of absolute FOIs and extract secondary features, such as integrals between a voltage interval or focus on DVA only.

4.3. Transfer from cell to vehicle

In this section, transferability of DVA and ICA from cell to vehicle level application is examined. Hereby, a similar charging process and C-rate is set up for a fair comparison between cell to vehicle level measurements. In Fig. 6(a) and (d) the vehicles' voltage curves are overlaid onto the voltage curves of the respective cells and additionally shifted by matching the vehicles' lowest sampled voltage value. The shift is necessary for a direct comparison of FOIs, as most notably the lower cut-off voltage differs between the vehicles and cells. Safety functions running on the BMS presumably limit the voltage to fall below a threshold of approx. 360 V for the VW and approx. 330 V for the Tesla to possibly mitigate deep discharging. The constant shift can be used to quantify the amount of retained charge which turns out to be 6.4 A h for the VW and 4.4 A h for the Tesla. The overlaid signals exhibit similar behaviors, although minor deviations are visible. Furthermore, the initial constant shift does not correct for any differences in the total capacity which is larger for the cell measurements in the laboratory.

The DV curves in Fig. 6(c) and (d) enable the examination of differences between the cell and vehicle level more closely. The FOIs in the shifted vehicle DV curves mostly coincide well in their positioning, but with less pronounced extrema. In terms of NE features, peak 3L in the VW's DV curve is difficult to detect on cell level and completely blurs out in the vehicle DV curve. The same holds for the 2L peak in both vehicles' DV curves. In VW's DV curve, stage 2 peak, important for determining the NE and balancing capacity, is not only lower in height, but also significantly shifted towards the left. The shift could indicate a lower amount of active material or overhang effects in the passive parts of the NE leading to shifts of FOIs [63,64]. The lower maxima is also observed by Reiter et al. [65] from DVA with cells in a module where they conclude that varying NE capacities between cells results in a module level stage 2 peak decrease. Furthermore, the distribution of the current between parallel cells induces inhomogeneity leading to the decrease and widening of this maxima [66,67]. As the Tesla has no parallel connections, this effect does nor occur. This could mean that battery packs with many parallel connected cells can be a disadvantage for diagnosis with DVA, where further measurements are necessary to underline this assumption.

Concerning PE features, the H2 peak in VW's DV curve is not precisely identifiable in height or position and can only be roughly estimated, similar as in the cell level DVA. No statements about PE FOIs can be made from DVA of the Tesla, as its LFP cell has no significant PE feature.

As IC curves are generally plotted against the directly measured voltage, shifting between cell and vehicle should not be necessary. VW's cell and vehicle IC curves in Fig. 6(e) align well and similar observations can be given as from DVA. Peak A and C are influenced by stage transitions in the graphite electrode showing a similar decrease of the extrema like the NE features from DVA. The maximum of peak B is difficult to resolve precisely due to the voltage resolution in this SOC regime but matches well with the cell level peak. Plateau D indicates processes in the PE matching well in position and height.

The IC curve of the Tesla in Fig. 6(f) exhibits a constant shift over the entire voltage signal. The cause of this offset is unknown, but could be due to summed measuring errors from the cells' voltage sensors or due to Ohmic resistances in the battery pack, e.g. connectors between the cells [50]. The latter can be estimated by a pseudo-resistance calculated by dividing the voltage difference of the peaks B by the applied current. This would result to approx. 200 mΩ on pack level or, considering two connectors per cells and two terminal connectors, a resistance of 0.95 mΩ between cells across laser welded aluminum bus bar connectors [49]. However, this value is higher than typical contact resistances for this manufacturing process [50] and presumably further resistances exist in the system. Canceling the shift leads to matching peak positions in the IC curves, except for peak A in the close-up showing differences in the NE which is comparable to the described effects discussed above for the VW. Comparing the heights of the remaining peaks is vacuous due to low data quality (see Section 4.2). The VW does not show this constant shift possibly due to lower Ohmic resistances of the connectors and a lower voltage drop across the parallel cell assembly.

From the findings above it can be concluded that it is possible to transfer both DVA and ICA onto the vehicle level which is the basis for potentially enabling battery pack SOH assessment similar to aging studies on the cell level, but limitations must be accepted. From DVA, insights into the electrodes are more accessible enabling the extraction of FOIs for deeper analysis of the battery's internal state. Peaks are detectable, but generally less pronounced. Nonetheless, the important stage 2 peak feature is clearly identifiable in both vehicles. Here, PE features from the VW DVA are difficult to extract due to this particular NMC composition. It is assumed that nickel-rich NMC compositions with generally more pronounced PE features leads to more visible FOIs on the vehicle level. Furthermore, parallel cells in battery packs dilute characteristics, with further experiments necessary to quantify this observation.

Furthermore, cell level measurements in the lab can be operated between larger voltage ranges than the cells in BEVs so that shifting is necessary to enables a comparison between BEV and cell level DV

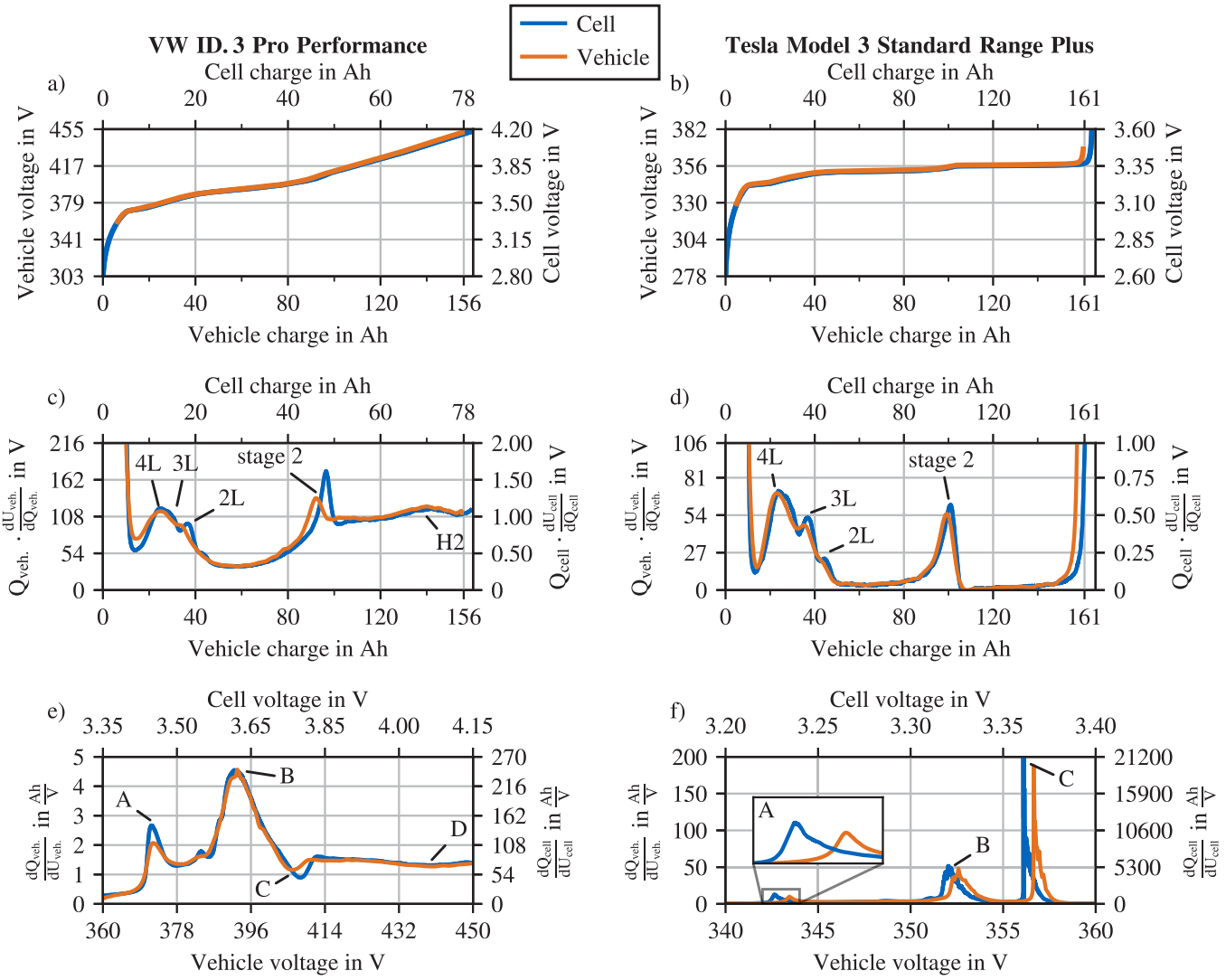

Fig. 6. Comparison of cell level to vehicle level measurements for both the VW (left column) and Tesla (right column). (a)/(b) Vehicle and cell level measurements with C-rates $^{C}/_{45}$ and $^{C}/_{57}$, respectively. (c)/(d) Vehicle and cell DV curves with labeled single phase stages. (e)/(f) Vehicle and cell IC curves with labeled stage transitions.

curves. For this, a reference must be defined, especially in prospect of deviations between measurements of multiple vehicles or for aligning DV curves from partial charging events. FOIs from ICA show similar findings as for DVA and matches well for the VW and Tesla. Alignment should not be required for IC curves as they are generally plotted against the voltage signal. However, the voltage can be influenced by secondary effects such as Ohmic resistances in the battery pack, that can lead to shifts which must be canceled out. All in all, there is no generally favorable method for BEV diagnostics, as both have their (dis-)advantages and should jointly be examined for analyzing the battery pack and extracting FOIs.

4.4. Aging

For analyzing vehicle level aging, the VW and Tesla are measured shortly after purchase and again after two years of usage with mileages of approx. 32 600 km and approx. 26 300 km, respectively. Despite the short period of time between the measurements, aging effects are captured as shown in Fig. 7. Hereby, the aged DV curve is aligned to the initial DV curve by the lowest recorded voltage.

The initial battery pack of the VW contains 60.6 kW h, whereas the aged measurement yields 55.0 kW h. Based on the net energy from Table 1, the SOH decreases from 104.4 % to 94.9 %. In terms of capacity this yields a loss of 12.1 A h which appears to be extreme considering the mileage. The energy storage capability of the Tesla reduces from 57.0 kW h to 55.1 kW h, equivalent to 108.6 % and 105.0 % SOH, respectively. This yields a capacity loss of 4.9 A h. It can be seen that even after this short time of usage, aging is present.

In Fig. 7(a) and (b), capacity loss is visible as a contraction of the aged DV curves. The electrode capacities are calculated as FOIs for DVA from the initial and aged measurement as shown in Fig. 2. The differences in electrode capacities are labeled in these figures and arrows indicate the shift direction to identify acting degradation modes.

The NE capacities Q_{NE} slightly change in both vehicles and even increases for the VW. Therefore, no significant loss of NE capacity or loss of active material at the negative electrode (LAM_{NE}) is assumed at these mileages which fits cell level aging studies with comparable stress factors [21,68]. The wider stage 2 peak can be due to different inhomogeneity levels of the NE [20]. It can also be an indicator for calendar aging effects [69], which generally fits the usage of private

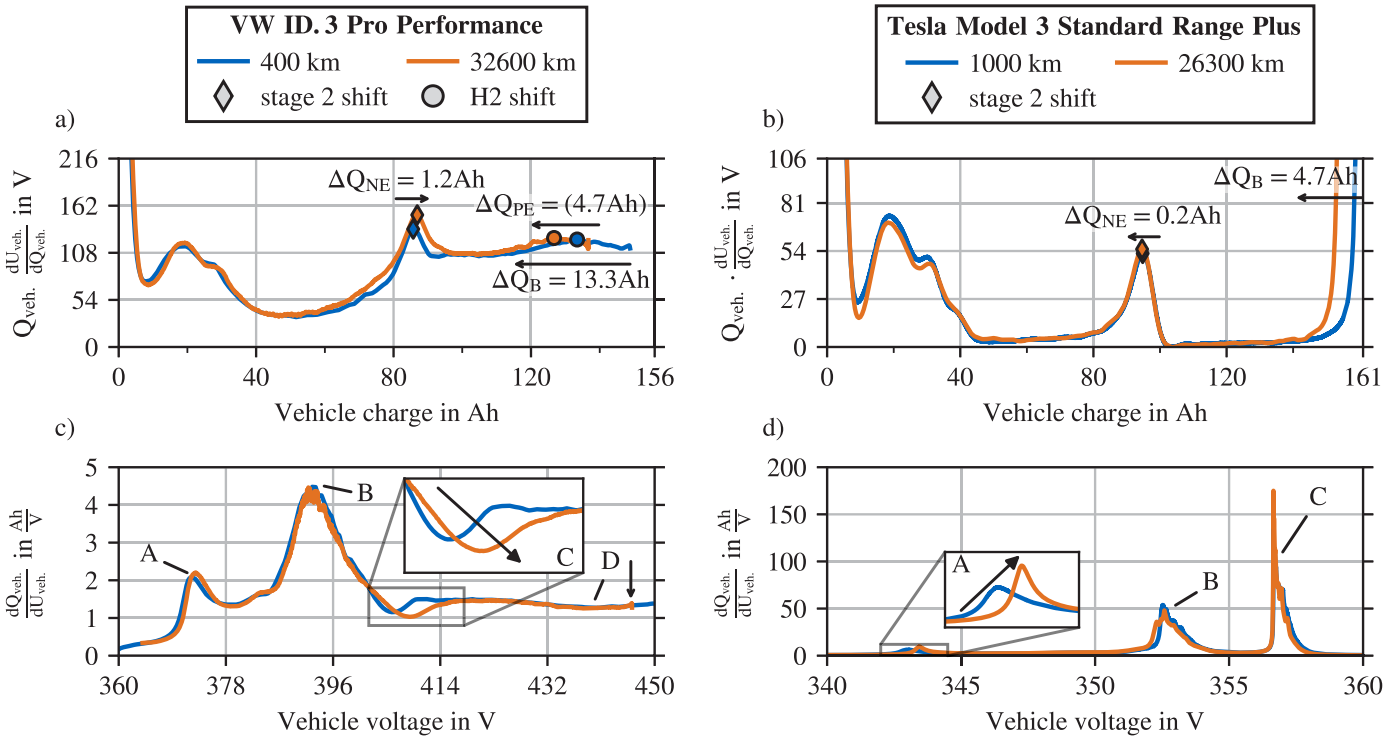

Fig. 7. Comparison of an initial measurement from the VW (left column) and Tesla (right column) with a measurement after two years of usage. (a)/(b) Comparison of vehicle DVAs from the initial and aged vehicle state. The difference in the capacities ΔQ_{NE}, ΔQ_{PE} and ΔQ_B are labeled and the direction of the peak shifts indicated. (c)/(d) Comparison of vehicle IC curves from the initial and aged vehicle state. The stage transitions are labeled. The close up plots magnify the only changing FOI. The upper cut-off voltage in the VW was restricted during the aged measurement, which is indicated by the vertical arrow. The lower part of the voltage signal is cropped for better visibility, due to numerical oscillations.

passenger cars that are mostly parked [70]. Hereby, the PE's M phase shifts towards the left below the stage 2 peak increasing its height, as a result of LLI. Coherently, this cannot be observed for the Tesla with no PE FOI.

A change of the PE capacity observed from the VW DVA is difficult to extract as the H2 peak is not clearly pronounced and superimposed by numerically caused oscillations. The peak is evaluated to the best of our ability indicating loss of active material at the positive electrode (LAM_{PE}) of $\Delta Q_{PE} \approx 4.7$ A h. However, the voltage window of the VW measurement, seen in Fig. 7(c), shows that the upper cut-off voltage is restricted compared to the initial measurement indicated by the vertical arrow, presumably by the BMS and possibly as a safety measure to restrict impermissible operating conditions. This restriction could also be seen in repeated measurements and is likely also responsible for a decrease of available capacity. This in turn would also affect the extraction of the capacity feature Q_{PE}. Cross-validating by additionally considering FOIs from ICA provides clarity. Hereby, degradation maps from Dubarry and Ansean [18] give insight of peak evolution from a graphite/NMC532 cell comparable to the cell chemistry in the VW that gives the following interpretation. LAM_{PE} can be excluded as the valley feature D stays the same. Hence, $\Delta Q_{PE} \approx 0$ A h is more realistic, meaning this feature is falsely altered due to BMS interference. It is more probable, but can only be assumed, that the shift ΔQ_{PE} actually resembles LLI but falsely indicates LAM_{PE} given the Q_{PE} feature definition. Hence, the VW most likely lost 3.5 A h (+1.2 A h–4.7 A h), which is in a similar range as the Tesla. This yields a more realistic SOH estimate of 101.6 %, and 8.6 A h could have been further charged if the same upper cut-off voltage had been reached.

The voltage limits do not change in the Tesla, but a PE capacity cannot be evaluated from DVA, due to the lack of a PE feature. Though similar findings from ICA can be compared to a LFP degradation map [18]. LAM_{PE} can be excluded as peak A shifts to the right and upwards while peaks B and C stay the same [18].

The most significant change within both vehicles can be assigned to the electrode balancing capacity Q_B associated with loss of active lithium, either reversibly due to overhang effects in the NE and inhomogeneous lithiation or irreversibly by LLI, which are discussed more closely in the following.

During charging it can occur that charge is stored in the NE's overhang, unless the overhang is already full prior to the measurement. Comparing measurements with full and empty overhangs then falsely appears as a loss/gain of capacity [67]. The share of overhang effects in the NE on the total loss of active lithium can only be estimated, but is assumed to play a minor role as the passive area of the NE only makes up 2.5 % in the VW [37] and 7.3 % in the Tesla [49] whereas the overhang is furthermore only partially lithiated [64]. It remains unclear if overhang effects are measurable on vehicle level as it acts on a significantly smaller scale than the active electrode area in these large format LIB cells. Further vehicle measurements are therefore necessary to quantify this statement.

This means the majority of irreversible capacity loss is attributable to LLI. The same statement can be given by tracking the evolution of peaks by ICA. Peak A in VW's IC curve is sensitive to LLI and LAM_{PE}, whereas the latter is already excluded from the previous findings. Therefore, the slight shift of the peak towards higher voltages indicates LLI. If LAM_{NE} can be excluded, e.g. here by DVA, then the shift of feature C in VW's IC curve towards higher voltages is also attributable to LLI. The ICA of the Tesla shows that only the first peak shifts towards higher voltages which strongly correlates with LLI. Furthermore, the

inner resistance increase can be neglected for both vehicles as no constant shift between IC curves is detectable.

All in all, it can be assumed that LLI is the main degradation mode for actual irreversible capacity loss. This aligns well with cell aging studies in literature [21,68], as the growth of passivation layers like SEI predominantly takes place at an early stage of aging and directly causes LLI. However, here, LLI is not the sole reason for the total loss of capacity.

This examination shows that it is possible to extract FOIs from vehicle level DVA and ICA that have thoroughly been investigated by cell level aging studies in literature. However, secondary influence superimpose irreversible aging such as interference of the BMS that can alter FOIs, as shown for the capacity feature Q_{PE}. Therefore, it is challenging to precisely disaggregate all effects of capacity loss especially when only examining either DVA or ICA. Here, a coherent picture could be created by a joint analysis of both DVA and ICA.

In the case of the VW, the estimated SOH might be close to the actual net energy of the battery pack but no longer coincides with the achievable range of the vehicle due to the voltage restrictions. The latter is, however, the more relevant parameter for a vehicle operator or fleet manager. Nonetheless, vehicle level battery diagnosis with DVA and ICA holds great potential for battery pack diagnosis during charging and further research is necessary, especially for evaluating reproducible FOIs which might only be suitable for statistical SOH models, e.g. machine learning.

Despite the disadvantages and limitations of vehicle level DVA and ICA, a diagnostic charging cycle is proposed. Assuming LLI is the dominant degradation mode in BEVs, which is likely throughout the first years of usage, then it is sufficient to partially charge the vehicles with a low C-rate from a mid-range SOC around 50 % SOC to the upper cut-off voltage at 100 % SOC (assuming the upper cut-off voltage does not change). Capturing the voltage curve in this interval and performing DVA makes it possible to extract the balancing feature Q_B which correlates with LLI. An advantage of partial charging sessions is the simple implementation and applicability in real world usage scenarios as BEVs must regularly be charged, often many hours over night. Performing this diagnostic charging procedure in periodic intervals makes it possible to quantify and track the evolution of Q_B over time from DVA, as the stage 2 peak has been detectable throughout all measurements. In addition, ICA can be used for cross validation, especially when voltage boundaries change. Nevertheless, if LAM occurs, it must be ensured that both a NE and PE feature can be detected, and charging through a wider SOC range is necessary.

4.5. BMS software versions

After the charging measurements discussed in Section 4.4 were conducted, VW announced that the ID.3 under test would be updated to ID.Software version 3.2. The General German Automobile Association (ADAC) conducted experiments with this software version, observing a different behavior in battery pack applications so that it can be assumed that the BMS software is also updated [71]. VW themselves do not disclose precise changes made [72]. The proposed measurement procedure was repeated after the update to analyze potential effects on the battery pack. A chronology of the VW's software versions and underlying measurement dates are given in the Appendix in Table 2. From this measurement, it could be seen that the upper voltage restriction discussed in Section 4.4 was lifted, and more capacity could be charged into the battery pack, shown in Fig. 8, yielding a transferred energy of 59.40 kWh or an SOH of 102.5 %. Comparing this value to the derived SOH estimate from the joint assessment with DVA and ICA gives a deviation of 0.5 %, showing that a realistic SOH can be determined using vehicle level DVA and ICA despite external influences.

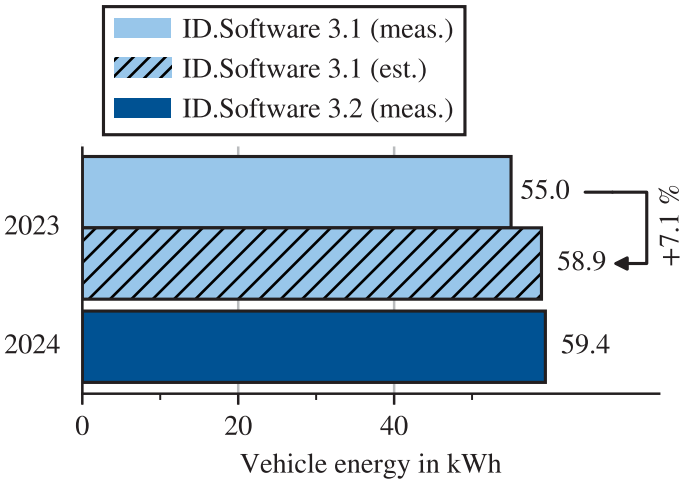

Fig. 8. Charged energy from measurements with different software versions. The SOH estimation technique explained in Section 4.4 yields a similar result as the measurement without a restricted upper cut-off voltage showing the robustness of a vehicle level SOH estimation with DVA and ICA.

5. Summary and conclusion

This study investigates the transferability of differential voltage and incremental capacity analysis from cell to vehicle level as an in-situ diagnostic method during charging. Both cell level, as well as vehicle measurements are conducted to compare similarities and differences in DVA and ICA. For the vehicle measurements, the two BEVs VW ID.3 and a Tesla Model 3 are measured during AC charging to capture the vehicle's voltage curve. Overall, DVA and ICA can successfully be performed on the vehicle level from charging measurements, however with limitations.

The data quality from the vehicles' on-board sensors is lower than in laboratory environments so that noise and the sensor resolution impede vehicle level DVA and ICA. Special care must be taken when filtering out noise from the signals so that FOI are not altered. ICA can be challenging, especially for LIBs with flat voltage profiles, as peaks in the IC curves stem from plateaus in the voltage curve that must be resolvable by the voltage sensor. It could be shown by lab measurements that a CP charging profile, common during AC charging of BEVs, does not prevent the use of DVA and ICA but marginally alters FOIs. The transferability of cell to vehicle level application is shown, as characteristic FOIs, such as peaks and valleys, are reproducible on the vehicle level, however less pronounced. This is especially visible for the battery pack of the VW, where the parallel connection of two cells in the battery pack dilute features, due to variations of NE capacities between cells in the battery pack and an inhomogeneous current distribution. A constant shift is notable between the IC curves of the Tesla compared to the cell level, possibly due to Ohmic resistances in the battery pack.

Vehicle measurements are performed shortly after purchase and again after a period of two years to analyze aging by DVA and ICA. Despite the rather short period of time, a significant reduction in SOH is detected. LLI, e.g. through SEI growth, seems to be the dominant aging mechanism in both vehicles, whereas overhang effects and BMS interference potentially also lead to a capacity reduction. Care must also be taken when BMS software versions are updated that can alter the behavior of the battery pack. Nonetheless, the evolution FOIs behaves similarly to findings in cell level aging studies. A diagnostic

cycle is proposed as it could be sufficient to detect LLI by partial charging between the stage 2 peak and the upper cut-off voltage between 50-100 % SOC to calculate the balancing feature Q_B for a SOH estimation.

6. Outlook

Further measurements are necessary to examine the robustness and generality of vehicle level DVA and ICA, e.g. by repeated measurements of the same vehicle or by conducting measurements in a fleet of a single vehicle model. Furthermore, LIBs are strongly influenced by external parameters, such as high C-rates and low temperatures which could be further examined on their effect on both methods.

The voltage across each serial cell in the battery pack assembly was additionally recorded during the measurements. Hence, it is also possible to calculate the DV and IC curves for each serial cell assembly inside the pack. This can enable an outlier detection for predictive maintenance use cases, e.g. locating faulty cells and scheduling workshop repairs [73].

In perspective of the next generation communication norms, open charge point protocol (OCPP) 2.0.1 [74] and ISO 15118-20 [75] will provide closer interaction between direct current (DC) charging stations and BEVs enabling the development of tailored diagnostic cycles [74, 76]. Thinkable are adapted charging cycles, e.g. sections of reduced power around certain FOIs or vehicle level HPPC to precisely extract FOI for an accurate SOH estimate.

CRediT authorship contribution statement

Philip Bilfinger: Writing – review & editing, Writing – original draft, Visualization, Methodology, Investigation, Formal analysis, Conceptualization. **Philipp Rosner:** Writing – review & editing, Methodology, Formal analysis. **Markus Schreiber:** Writing – review & editing, Methodology, Formal analysis. **Thomas Kröger:** Writing – review & editing, Methodology. **Kareem Abo Gamra:** Writing – review & editing, Methodology. **Manuel Ank:** Writing – review & editing, Methodology. **Nikolaos Wassiliadis:** Writing – review & editing, Methodology. **Brian Dietermann:** Writing – review & editing, Methodology. **Markus Lienkamp:** Writing – review & editing, Supervision, Resources, Funding acquisition.

Declaration of competing interest

The authors declare that they have no known competing financial interests or personal relationships that could have appeared to influence the work reported in this paper.

Data availability

We want to give any researcher access to our results without any limits. The data of all measurements can be found at mediaTUM. The code for processing the data is available at FTM Github.

Acknowledgments

This research received funding by the Bavarian Ministry of Economic Affairs, Regional Development and Energy, Germany within the project ‘charge.COM’ under the grant number DIK-0262/02 and ‘KiBaTest’ under the grant number DIK-0123/01. Furthermore, this work was partly funded by the German Federal Ministry for Economic Affairs and Climate Action (BMWK) within the project ‘ultraBatt’ under grant number 01MV21015D and German Federal Ministry of Education and Research (BMBF) within the projects ‘OptiPro’ under grant number 03XP0364B, ‘BALd’ under grant number 03XP0320B and ComfficientShare under grant number 03ZU1105CA.

Appendix A. Vehicle specifications

Table 1
Overview of battery pack and cell specifications from the VW and Tesla under study.

Domain	Attribute	VW	Tesla	Unit
Battery pack	Gross energy	62[a]	55[a]	kW h
	Net energy	58[a]	52.5[a]	kW h
	Voltage range	360–450[b]	330–380[e]	V
	Serial cells	108[b]	106[a]	–
	Parallel cells	2[b]	1[a]	–
Battery cell	Energy density	268[c]	163[d]	$W\,h\,kg^{-1}$
	Nom. capacity	78[c]	161.5[d]	A h
	Voltage range	2.8–4.2[c]	2.6–3.6[d]	V
	Cell format	pouch[c]	prismatic[d]	–
	Chemistry	C/NMC[c]	C/LFP[d]	–

[a] EV Database (VW [77], Tesla [48]).
[b] Wassiliadis et al. [2].
[c] Günter and Wassiliadis [37].
[d] Stock et al. [49].
[e] Measured data.

Appendix B. VW ID.3 software updates

Table 2
Chronology of the VW ID.3’s software updates and measurement dates. The software updates were applied during scheduled workshop stays.

Software version	Update	Measurement
ID.Software 2.0	2020-12-01	2021-02-08
ID.Software 2.1	2021-04-08	–
ID.Software 2.3	2021-11-04	–
ID.Software 2.4	2022-12-06	2023-06-16
ID.Software 3.2	2023-09-27	2024-05-22

References

[1] European Commission. A fundamental transport transformation: Commission presents its plan for green, smart and affordable mobility. 2020, visited on 05.12.2023, https://ec.europa.eu/commission/presscorner/detail/en/ip_20_2329.
[2] Wassiliadis N, Steinsträter M, Schreiber M, Rosner P, Nicoletti L, Schmid F, et al. Quantifying the state of the art of electric powertrains in battery electric vehicles: Range, efficiency, and lifetime from component to system level of the Volkswagen ID.3. eTransportation 2022;12:100167. http://dx.doi.org/10.1016/j.etran.2022.100167.
[3] Stroe D-I, Schaltz E. SOH estimation of LMO/NMC-based electric vehicle lithium-ion batteries using the incremental capacity analysis technique. IEEE Energy Convers Congr Expo 2018;2720–5. http://dx.doi.org/10.1109/ECCE.2018.8557998.
[4] Birkl CR, Roberts MR, McTurk E, Bruce PG, Howey DA. Degradation diagnostics for lithium ion cells. J Power Sources 2017;341:373–86. http://dx.doi.org/10.1016/j.jpowsour.2016.12.011.
[5] Vetter J, Novák P, Wagner MR, Veit C, Möller K-C, Besenhard JO, et al. Ageing mechanisms in lithium-ion batteries. J Power Sources 2005;147:269–81. http://dx.doi.org/10.1016/j.jpowsour.2005.01.006.
[6] Broussely M, Biensan P, Bonhomme F, Blanchard P, Herreyre S, Nechev K, et al. Main aging mechanisms in Li ion batteries. J Power Sources 2005;146:90–6. http://dx.doi.org/10.1016/j.jpowsour.2005.03.172.
[7] Keil P, Jossen A. Aging of lithium-ion batteries in electric vehicles: Impact of regenerative braking. World Electr Veh J 2015;7:41–51. http://dx.doi.org/10.3390/wevj7010041.
[8] Sulzer V, Mohtat P, Aitio A, Lee S, Yeh YT, Steinbacher F, et al. The challenge and opportunity of battery lifetime prediction from field data. Joule 2021;5:1934–55. http://dx.doi.org/10.1016/j.joule.2021.06.005.
[9] Peng J, Meng J, Chen D, Liu H, Hao S, Sui X, et al. A review of lithium-ion battery capacity estimation methods for onboard battery management systems: Recent progress and perspectives. Batteries 2022;8:229. http://dx.doi.org/10.3390/batteries8110229.
[10] Schaltz E, Stroe D-I, Norregaard K, Kofod L, Christensen A. Incremental capacity analysis for electric vehicle battery state-of-health estimation. Piscataway, NJ: IEEE; 2019, http://dx.doi.org/10.1109/EVER.2019.8813678.

[11] Schaltz E, Stroe D-I, Norregaard K, Ingvardsen LS, Christensen A. Incremental capacity analysis applied on electric vehicles for battery state-of-health estimation. IEEE Trans Ind Appl 2021;57:1810–7. http://dx.doi.org/10.1109/TIA.2021.3052454.

[12] Barai A, Uddin K, Dubarry M, Somerville L, McGordon A, Jennings P, et al. A comparison of methodologies for the non-invasive characterisation of commercial Li-ion cells. Prog Energy Combust Sci 2019;72:1–31. http://dx.doi.org/10.1016/j.pecs.2019.01.001.

[13] Bloom I, Jansen AN, Abraham DP, Knuth J, Jones SA, Battaglia VS, et al. Differential voltage analyses of high-power lithium-ion cells – 1. Technique and application. J Power Sources 2005;139:295–303. http://dx.doi.org/10.1016/j.jpowsour.2004.07.021.

[14] Bloom I, Christophersen J, Gering K. Differential voltage analyses of high-power lithium-ion cells – 2. Applications. J Power Sources 2005;139:304–13. http://dx.doi.org/10.1016/j.jpowsour.2004.07.022.

[15] Bloom I, Christophersen JP, Abraham DP, Gering KL. Differential voltage analyses of high-power lithium-ion cells – 3. Another anode phenomenon. J Power Sources 2006;157:537–42. http://dx.doi.org/10.1016/j.jpowsour.2005.07.054.

[16] Bloom I, Walker LK, Basco JK, Abraham DP, Christophersen JP, Ho CD. Differential voltage analyses of high-power lithium-ion cells – 4. Cells containing NMC. J Power Sources 2010;195:877–82. http://dx.doi.org/10.1016/j.jpowsour.2009.08.019.

[17] Fly A, Chen R. Rate dependency of incremental capacity analysis (dQ/dV) as a diagnostic tool for lithium-ion batteries. J Energy Storage 2020;29:101329. http://dx.doi.org/10.1016/j.est.2020.101329.

[18] Dubarry M, Anseán D. Best practices for incremental capacity analysis. Front Energy Res 2022;10. http://dx.doi.org/10.3389/fenrg.2022.1023555.

[19] Berecibar M, Garmendia M, Gandiaga I, Crego J, Villarreal I. State of health estimation algorithm of LiFePO4 battery packs based on differential voltage curves for battery management system application. Energy 2016;103:784–96. http://dx.doi.org/10.1016/j.energy.2016.02.163.

[20] Lewerenz M, Marongiu A, Warnecke A, Sauer DU. Differential voltage analysis as a tool for analyzing inhomogeneous aging: A case study for LiFePO4|Graphite cylindrical cells. J Power Sources 2017;368:57–67. http://dx.doi.org/10.1016/j.jpowsour.2017.09.059.

[21] Wildfeuer L, Karger A, Aygül D, Wassiliadis N, Jossen A, Lienkamp M. Experimental degradation study of a commercial lithium-ion battery. J Power Sources 2023;560:232498. http://dx.doi.org/10.1016/j.jpowsour.2022.232498.

[22] Wang L, Zhao X, Liu L, Pan C. State of health estimation of battery modules via differential voltage analysis with local data symmetry method. Electrochim Acta 2017;256:81–9. http://dx.doi.org/10.1016/j.electacta.2017.10.025.

[23] Baumann M, Wildfeuer L, Rohr S, Lienkamp M. Parameter variations within Li-Ion battery packs – Theoretical investigations and experimental quantification. J Energy Storage 2018;18:295–307. http://dx.doi.org/10.1016/j.est.2018.04.031.

[24] Ank M, Stock S, Wassiliadis N, Burger T, Daub R, Lienkamp M. Influence analysis of production defects of lithium-ion cells using single-cell and multi-cell characterization. J Energy Storage 2023;62:106938. http://dx.doi.org/10.1016/j.est.2023.106938.

[25] Sun S, Zhang H, Ge J, Che L. State-of-health estimation for lithium-ion battery using model-based feature optimization and deep extreme learning machine. J Energy Storage 2023;72:108732. http://dx.doi.org/10.1016/j.est.2023.108732.

[26] Schmitt J, Rehm M, Karger A, Jossen A. Capacity and degradation mode estimation for lithium-ion batteries based on partial charging curves at different current rates. J Energy Storage 2023;59:106517. http://dx.doi.org/10.1016/j.est.2022.106517.

[27] Weng C, Feng X, Sun J, Peng H. State-of-health monitoring of lithium-ion battery modules and packs via incremental capacity peak tracking. Appl Energy 2016;180:360–8. http://dx.doi.org/10.1016/j.apenergy.2016.07.126.

[28] Krupp A, Ferg E, Schuldt F, Derendorf K, Agert C. Incremental capacity analysis as a state of health estimation method for lithium-ion battery modules with series-connected cells. Batteries 2020. http://dx.doi.org/10.3390/batteries7010002.

[29] Rosenberger N, Rosner P, Bilfinger P, Schöberl J, Teichert O, Schneider J, et al. Quantifying the state of the art of electric powertrains in battery electric vehicles: Comprehensive analysis of the tesla model 3 on the vehicle level. World Electr Veh J 2024;15(6):268. http://dx.doi.org/10.3390/wevj15060268.

[30] She C, Wang Z, Sun F, Liu P, Zhang L. Battery aging assessment for real-world electric buses based on incremental capacity analysis and radial basis function neural network. IEEE Trans Ind Inf 2020;16:3345–54. http://dx.doi.org/10.1109/TII.2019.2951843.

[31] She C, Zhang L, Wang Z, Sun F, Liu P, Song C. Battery state of health estimation based on incremental capacity analysis method: Synthesizing from cell-level test to real-world application. IEEE J Emerg Sel Top Power Electron 2021. http://dx.doi.org/10.1109/JESTPE.2021.3112754.

[32] Dubarry M, Svoboda V, Hwu R, Yann Liaw B. Incremental capacity analysis and close-to-equilibrium OCV measurements to quantify capacity fade in commercial rechargeable lithium batteries. Electrochem Solid-State Lett 2006;9:A454. http://dx.doi.org/10.1149/1.2221767.

[33] Schweidler S, de Biasi L, Schiele A, Hartmann P, Brezesinski T, Janek J. Volume changes of graphite anodes revisited: A combined operando X-ray diffraction and in situ pressure analysis study. J Phys Chem C 2018;122:8829–35. http://dx.doi.org/10.1021/acs.jpcc.8b01873.

[34] Dühnen S, Betz J, Kolek M, Schmuch R, Winter M, Placke T. Toward green battery cells: Perspective on materials and technologies. Small Methods 2020;4. http://dx.doi.org/10.1002/smtd.202000039.

[35] Jung R, Metzger M, Maglia F, Stinner C, Gasteiger HA. Oxygen release and its effect on the cycling stability of LiNixMnyCozO2 (NMC) cathode materials for li-ion batteries. J Electrochem Soc 2017;164:A1361–77. http://dx.doi.org/10.1149/2.0021707jes.

[36] Dolotko O, Senyshyn A, Mühlbauer M, Nikolowski K, Ehrenberg H. Understanding structural changes in NMC Li-ion cells by in situ neutron diffraction. J Power Sources 2014;255:197–203. http://dx.doi.org/10.1016/j.jpowsour.2014.01.010.

[37] Günter FJ, Wassiliadis N. State of the art of lithium-ion pouch cells in automotive applications: Cell teardown and characterization. J Electrochem Soc 2022. http://dx.doi.org/10.1149/1945-7111/ac4e11.

[38] Ank M, Sommer A, Abo Gamra K, Schöberl J, Leeb M, Schachtl J, et al. Lithium-ion cells in automotive applications: Tesla 4680 cylindrical cell teardown and characterization. J Electrochem Soc 2023;170:120536. http://dx.doi.org/10.1149/1945-7111/ad14d0.

[39] Simolka M, Heger J-F, Traub N, Kaess H, Friedrich KA. Influence of cycling profile, depth of discharge and temperature on commercial LFP/C cell ageing: Cell level analysis with ICA, DVA and OCV measurements. J Electrochem Soc 2020;167:110502. http://dx.doi.org/10.1149/1945-7111/ab9cd1.

[40] Dubarry M, Devie A, Liaw BY. The value of battery diagnostics and prognostics. J Energy Power Sources 2014. visited on 15.02.2024.

[41] Dubarry M, Truchot C, Liaw BY. Synthesize battery degradation modes via a diagnostic and prognostic model. J Power Sources 2012;219:204–16. http://dx.doi.org/10.1016/j.jpowsour.2012.07.016.

[42] Smith AJ, Dahn JR. Delta differential capacity analysis. J Electrochem Soc 2012;159:290–3. http://dx.doi.org/10.1149/2.076203jes.

[43] Danko M, Adamec J, Taraba M, Drgona P. Overview of batteries State of Charge estimation methods. Transp Res Procedia 2019;40:186–92. http://dx.doi.org/10.1016/j.trpro.2019.07.029.

[44] Li Y, Abdel-Monem M, Gopalakrishnan R, Berecibar M, Nanini-Maury E, Omar N, et al. A quick on-line state of health estimation method for Li-ion battery with incremental capacity curves processed by Gaussian filter. J Power Sources 2018;373:40–53. http://dx.doi.org/10.1016/j.jpowsour.2017.10.092.

[45] Carter R, Kingston TA, Atkinson RW, Parmananda M, Dubarry M, Fear C, et al. Directionality of thermal gradients in lithium-ion batteries dictates diverging degradation modes. Cell Rep Phys Sci 2021;2:100351. http://dx.doi.org/10.1016/j.xcrp.2021.100351.

[46] Guo J, Li Y, Meng J, Pedersen K, Gurevich L, Stroe D-I. Understanding the mechanism of capacity increase during early cycling of commercial NMC/graphite lithium-ion batteries. J Energy Chem 2022;74:34–44. http://dx.doi.org/10.1016/j.jechem.2022.07.005.

[47] Jenu S, Hentunen A, Haavisto J, Pihlatie M. State of health estimation of cycle aged large format lithium-ion cells based on partial charging. J Energy Storage 2022;46:103855. http://dx.doi.org/10.1016/j.est.2021.103855.

[48] Electric Vehicle Database. Tesla Model 3 Standard Plus LFP. visited on 14.02.2024, https://ev-database.org/de/pkw/1320/Tesla-Model-3-Standard-Plus-LFP.

[49] Stock S, Hagemeister J, Grabmann S, Kriegler J, Keilhofer J, Ank M, et al. Cell teardown and characterization of an automotive prismatic LFP battery. Electrochim Acta 2023;471:143341. http://dx.doi.org/10.1016/j.electacta.2023.143341.

[50] Wassiliadis N, Ank M, Wildfeuer L, Kick MK, Lienkamp M. Experimental investigation of the influence of electrical contact resistance on lithium-ion battery testing for fast-charge applications. Appl Energy 2021;295:117064. http://dx.doi.org/10.1016/j.apenergy.2021.117064.

[51] Juice Technology AG. Juice Booster 2. visited on 14.02.2024, https://juice.world/produkte/juice-booster-2/.

[52] Jossen A, Weydanz W. Moderne Akkumulatoren richtig einsetzen. 2nd ed. Göttingen: MatrixMedia Verlag; 2021, isbn: 978-3-946891-18-5.

[53] Iurilli P, Brivio C, Merlo M. SoC management strategies in battery energy storage system providing primary control reserve. Sustain Energy Grids Netw 2019;19:100230. http://dx.doi.org/10.1016/j.segan.2019.100230.

[54] Wardell J. Tesla Model 3 .dbc file, github repository. 2021, visited on 15.02.2024, https://github.com/joshwardell/model3dbc.

[55] Schmid F. UDS Decoder, GitHub repository. 2022, visited on 14.02.2024, https://github.com/TUMFTM/uds-decoder/.

[56] Merkle L, Pöthig M, Schmid F. Estimate E-golf battery state using diagnostic data and a digital twin. Batteries 2021;7:15. http://dx.doi.org/10.3390/batteries7010015.

[57] Kalogiannis T, Stroe DI, Nyborg J, Nø rregaard K, Christensen AEr, Schaltz E. Incremental capacity analysis of a lithium-ion battery pack for different charging rates. ECS Trans 2017;77:403–12. http://dx.doi.org/10.1149/07711.0403ecst.

[58] Anseán D, Dubarry M, Devie A, Liaw BY, García VM, Viera JC, et al. Fast charging technique for high power LiFePO4 batteries: A mechanistic analysis of aging. J Power Sources 2016;321:201–9. http://dx.doi.org/10.1016/j.jpowsour.2016.04.140.

[59] Liu P, Wu Y, She C, Wang Z, Zhang Z. Comparative study of incremental capacity curve determination methods for lithium-ion batteries considering the real-world situation. IEEE Trans Power Electron 2022;37:12563–76. http://dx.doi.org/10.1109/TPEL.2022.3173464.

[60] Koltypin M, Aurbach D, Nazar L, Ellis B. On the stability of LiFePO olivine cathodes under various conditions (electrolyte solutions, temperatures). Electrochem Solid-State Lett 2007;10:A40. http://dx.doi.org/10.1149/1.2403974.

[61] Koltypin M, Aurbach D, Nazar L, Ellis B. More on the performance of LiFePO4 electrodes—The effect of synthesis route, solution composition, aging, and temperature. J Power Sources 2007;174:1241–50. http://dx.doi.org/10.1016/j.jpowsour.2007.06.045.

[62] Smith SW. The scientist and engineer's guide to digital signal processing. California Technical Pub; 1997, isbn: 978-0-966017-63-2.

[63] Fath JP, Dragicevic D, Bittel L, Nuhic A, Sieg J, Hahn S, et al. Quantification of aging mechanisms and inhomogeneity in cycled lithium-ion cells by differential voltage analysis. J Energy Storage 2019;25:100813. http://dx.doi.org/10.1016/j.est.2019.100813.

[64] Fath JP, Alsheimer L, Storch M, Stadler J, Bandlow J, Hahn S, et al. The influence of the anode overhang effect on the capacity of lithium-ion cells – a 0D-modeling approach. J Energy Storage 2020;29:101344. http://dx.doi.org/10.1016/j.est.2020.101344.

[65] Reiter A, Lehner S, Bohlen O, Sauer DU. Electrical cell-to-cell variations within large-scale battery systems — A novel characterization and modeling approach. J Energy Storage 2023;57:106152. http://dx.doi.org/10.1016/j.est.2022.106152.

[66] Lewerenz M, Sauer DU. Evaluation of cyclic aging tests of prismatic automotive LiNiMnCoO2-graphite cells considering influence of homogeneity and anode overhang. J Energy Storage 2018;18:421–34. http://dx.doi.org/10.1016/j.est.2018.06.003.

[67] Lewerenz M, Fuchs G, Becker L, Sauer DU. Irreversible calendar aging and quantification of the reversible capacity loss caused by anode overhang. J Energy Storage 2018;18:149–59. http://dx.doi.org/10.1016/j.est.2018.04.029.

[68] Schreiber M, Abo Gamra K, Bilfinger P, Teichert O, Schneider J, Kröger T, et al. Understanding lithium-ion battery degradation in vehicle applications: Insights from realistic and accelerated aging tests using Volkswagen ID.3 pouch cells. 2024, preprint available https://papers.ssrn.com/sol3/papers.cfm?abstract_id=4911103.

[69] Keil P, Jossen A. Calendar aging of NCA lithium-ion batteries investigated by differential voltage analysis and Coulomb tracking. J Electrochem Soc 2017;164:6066–74. http://dx.doi.org/10.1149/2.0091701jes.

[70] Leibling JBD, Bayliss D. Spaced out-perspectives on parking policy. 2012, visited on 15.02.2024, https://www.racfoundation.org/wp-content/uploads/2017/11/spaced_out-bates_leibling-jul12.pdf.

[71] Wieler J. ID.Software 3.2 Test, ADAC. 2024, visited on 09.07.2024, https://www.adac.de/rund-ums-fahrzeug/ausstattung-technik-zubehoer/assistenzsysteme/vw-id3-software-update/.

[72] VW. ID.Software 3.2. 2023, visited on 09.07.2024, https://www.vw.com/en/owners-and-services/connectivity-and-apps/vehicle-software-updates/electric-vehicle-software-updates/electric-vehicle-software-update-3-2.html.

[73] Ank M, Brehler T, Lienkamp M. Wire bond contact defect identification in battery modules of electric vehicles using pulses and differential voltage analysis. eTransportation 2023;18:100284. http://dx.doi.org/10.1016/j.etran.2023.100284.

[74] Buve F, Klapwijk P, de Leeuw R. OCPP 2.0.1 Protocol Description. 2020, visited on 14.02.2024, https://openchargealliance.org/protocols/open-charge-point-protocol/.

[75] Heinrich A, Schwaiger M. ISO 15118 – charging communication between plug-in electric vehicles and charging infrastructure. 2017, p. 213–27, isbn: 978-3-658-15443-1,

[76] Nationale Plattform Zukunft der Mobilität. Roadmap zur Implementierung der ISO 15118: Standardisierte Kommunikation zwischen Fahrzeug und Ladepunkt. 2020, visited on 14.02.2024, https://www.plattform-zukunft-mobilitaet.de/2download/roadmap-zur-implementierung-der-iso-15118-standardisierte-kommunikation-zwischen-fahrzeug-und-ladepunkt/,

[77] Electric Vehicle Database. Volkswagen ID.3 Pro Performance. visited on 14.02.2024, https://ev-database.org/de/pkw/1831/Volkswagen-ID3-Pro.